

# Ferromagnetic fluctuation and possible triplet superconductivity due to the inter-orbital Hund's-rule coupling in $\text{Na}_{0.35}\text{CoO}_2 \cdot 1.3\text{H}_2\text{O}$ : FLEX study of the multi-orbital Hubbard model

Masahito Mochizuki, Youichi Yanase and Masao Ogata

Department of Physics, University of Tokyo, Hongo Bunkyo-ku Tokyo 113-0033, Japan

(Dated: today)

Spin and charge fluctuations and superconductivity in a recently discovered superconductor  $\text{Na}_{0.35}\text{CoO}_2 \cdot 1.3\text{H}_2\text{O}$  are studied based on a multi-orbital Hubbard model. Tight-binding parameters are determined to reproduce the LDA band dispersions with the Fermi surfaces, which consist of a large cylindrical one around  $\Gamma$ -point and six hole pockets near the K-points. By applying the fluctuation exchange (FLEX) approximation, we show that the Hund's-rule coupling between the Co  $t_{2g}$  orbitals causes ferromagnetic (FM) spin fluctuation. Triplet  $f_{y(y^2-3x^2)}$ -wave and  $p$ -wave pairings are favored by this FM fluctuation on the hole-pocket band. We propose that, in  $\text{Na}_{0.35}\text{CoO}_2 \cdot 1.3\text{H}_2\text{O}$ , Co  $t_{2g}$  orbitals and inter-orbital Hund's-rule coupling play important roles on the triplet pairing, and this compound can be a first example of the triplet superconductor mediated by inter-orbital-interaction-induced FM fluctuation.

PACS numbers: 74.20.Mn

Recently, the first Co-based oxide superconductor  $\text{Na}_{0.35}\text{CoO}_2 \cdot 1.3\text{H}_2\text{O}$  with  $T_c \sim 5$  K was discovered by Takada *et al.* [1]. In this compound, edge shared  $\text{CoO}_6$  octahedra form  $\text{CoO}_2$  planes similar to the high  $T_c$  cuprates with  $\text{CuO}_2$  planes. However, Co ions form a triangular lattice in the  $\text{CoO}_2$  plane. It is also remarkable that the enhancement of two dimensionality by water intercalation induces superconductivity. Mechanisms and nature of the superconductivity are currently attracting great interest because of a possible realization of resonating-valence bond (RVB) state proposed by Anderson [2, 3] in a triangular lattice. Although there are still some controversies, extensive Co NMR/NQR experiments have shown evidences for non- $s$ -wave superconductivity [4, 5, 6]. Furthermore, various experiments on the non-water-intercalated compounds show characteristic behaviors of strongly correlated electron systems [7, 8]. In spite of these extensive studies, however, the pairing symmetry has not been determined.

From theoretical viewpoints, this compound has several interesting features. One is geometrical frustration due to the triangular lattice and another is the degeneracy of Co  $3d$  orbitals. Originally, the RVB state was proposed in the Heisenberg model on a triangular lattice. Actually high-temperature expansion study suggests that the carrier doping to the triangular Heisenberg model induces RVB superconductivity [9]. Recent mean-field analyses of  $t$ - $J$  model have shown that chiral  $d_{xy} + id_{x^2+y^2}$ -wave superconductivity is stabilized [10, 11, 12, 13]. However, the broken time-reversal symmetry has not been observed so far [14], and alternative states have been investigated.

According to the triangular crystal symmetry, superconducting states are classified as  $s$ -,  $p$ -,  $d$ -,  $f_{x(x^2-3y^2)}$  (or next-nearest-neighbor  $f$ -),  $f_{y(y^2-3x^2)}$ , and  $i$ -wave pairings. Previous microscopic theories using various model Hamiltonians have shown that various symmetries arise depending on the model. For example, if one uses an extended Hubbard model which has a charge-

ordering instability in large- $V$  region [15, 16], one obtains the next-nearest-neighbor  $f$ -wave superconductivity [19]. On the other hand, in the single-band Hubbard model,  $d_{xy} + id_{x^2+y^2}$ - and  $f$ -wave states are obtained [17, 18]. We think that this variety of superconducting states is due to frustration which does not give any specific momentum dependence of  $\chi_s(q)$ .

The above theories, however, assumed a single-band model. As shown by LDA calculations [20, 21], there is apparently an orbital degeneracy in  $\text{Na}_x\text{CoO}_2$  systems. Actually two bands constructed from the three Co  $t_{2g}$  orbitals intersect the Fermi level. Furthermore, the electron fillings of these two bands are far from half filling. This means that in this material multi bands (in other words, multi orbitals) contribute to low-energy electronic structure. This is in marked contrast with the high- $T_c$  cuprates.

In this letter, we study the electronic structure and superconductivity in  $\text{Na}_{0.35}\text{CoO}_2 \cdot 1.3\text{H}_2\text{O}$  on the basis of the multi-orbital Hubbard model, which includes the Co  $t_{2g}$  orbitals and the inter- and intra-orbital interactions. We find that several important and interesting aspects appear which were not expected in the single-band model. One of them is a ferromagnetic (FM) spin fluctuation which appears from the six hole pockets consisting of  $e'_g$  orbitals as described below, and which is enhanced by the inter-orbital Hund's-rule coupling. Actually, an evidence for the FM fluctuation has been observed by Co-NQR experiments in several groups [4, 5, 22] and expected in the LSDA calculation [23]. We will show that this FM spin fluctuation leads to triplet pairing mainly on the hole pockets in contrast with the naive expectation of the RVB superconductivity in the single-band  $t$ - $J$  model. Here, the disconnectivity of the Fermi surface plays an important role. First, we will deduce the tight-binding parameters which reproduce the LDA band dispersions [20, 21]. Then we apply the fluctuation exchange (FLEX) approximation to this multi-orbital Hubbard model. Generally speaking, the FLEX

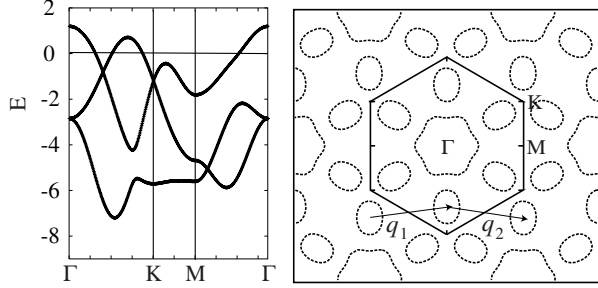


FIG. 1: Band dispersions (left panel) and Fermi surfaces (right panel) obtained from  $H_{\text{kin.}} + H_{\text{cry.}}$ . Both reproduce very well the characters of the LDA results [Ref. [20]], especially near the Fermi level.

calculation is appropriate in the case near a quantum critical point because the critical enhancement of fluctuation can be taken into account. We point out that  $\text{Na}_{0.35}\text{CoO}_2 \cdot 1.3\text{H}_2\text{O}$  can provide a first example of the triplet superconductivity which clarifies the important roles of orbitals on the superconductivity in the strongly correlated electron systems.

We study the multi-orbital Hamiltonian given by  $H = H_{\text{cry.}} + H_{\text{kin.}} + H_{\text{int.}}$  with  $H_{\text{cry.}} = \sum_{i,m,n,\sigma} D_{mn} d_{im\sigma}^\dagger d_{in\sigma}$ ,  $H_{\text{kin.}} = \sum_{i,j,m,n,\sigma} t_{ij}^{mn} d_{im\sigma}^\dagger d_{jn\sigma} - \mu \sum_{i,m,\sigma} d_{im\sigma}^\dagger d_{im\sigma}$ , and  $H_{\text{int.}} = H_U + H_{U'} + H_{J_H} + H_{J'}$ , where  $d_{im\sigma}$  ( $d_{im\sigma}^\dagger$ ) is the annihilation (creation) operator of an electron with spin  $\sigma$  ( $=\uparrow, \downarrow$ ) in the orbital  $m$  on the Co site  $i$ . Here,  $m$  runs over the  $xy$ ,  $yz$ , and  $zx$  orbitals. The first term  $H_{\text{cry.}}$  expresses the crystal field from the O ions acting on the Co  $t_{2g}$  orbitals. In  $\text{Na}_{0.35}\text{CoO}_2 \cdot 1.3\text{H}_2\text{O}$ , the  $\text{CoO}_6$  octahedron is contracted along the  $c$ -axis. The ligand oxygens on the  $\text{CoO}_6$  octahedron with this distortion generate a trigonal crystal field, and the matrix element of  $D_{mn}$  is given by  $\frac{\Delta}{3}(1 - \delta_{mn})$ . This crystal field lifts the local  $t_{2g}$  degeneracy into lower  $a_{1g}$  and higher  $e'_g$  levels with energy splitting of  $\Delta$ .

The second term  $H_{\text{kin.}}$  represents the kinetic-energy. Here,  $\mu$  is the chemical potential, and  $t_{ij}^{mn}$  is the hopping integral between the  $m$  orbital on the  $i$  site and the  $n$  orbital on the  $j$  site. In order to reproduce the LDA [20] band structures, we find that up to the third nearest-neighbor hoppings between orbitals are necessary. In the  $k$ -space,  $H_{\text{kin.}}$  is rewritten as  $H_{\text{kin.}} = \sum_{\mathbf{k},m,n,\sigma} \epsilon_{\mathbf{k}}^{mn} d_{\mathbf{k}m\sigma}^\dagger d_{\mathbf{k}n\sigma} - \mu \sum_{\mathbf{k},m,\sigma} d_{\mathbf{k}m\sigma}^\dagger d_{\mathbf{k}m\sigma}$  with

$$\begin{aligned} \epsilon_{\mathbf{k}}^{\gamma\gamma} &= 2t_1 \cos k_a^{\gamma\gamma} + 2t_2 [\cos k_b^{\gamma\gamma} + \cos(k_a^{\gamma\gamma} + k_b^{\gamma\gamma})] \\ &+ 2t_4 [\cos(2k_a^{\gamma\gamma} + k_b^{\gamma\gamma}) + \cos(k_a^{\gamma\gamma} - k_b^{\gamma\gamma})] + 2t_5 \cos 2k_a^{\gamma\gamma}, \\ \epsilon_{\mathbf{k}}^{\gamma\gamma'} &= 2t_3 \cos k_b^{\gamma\gamma'} + 2t_6 \cos 2k_b^{\gamma\gamma'} + 2t_7 \cos(k_a^{\gamma\gamma'} + 2k_b^{\gamma\gamma'}) \\ &+ 2t_8 \cos(k_a^{\gamma\gamma'} - k_b^{\gamma\gamma'}) + 2t_9 \cos(2k_a^{\gamma\gamma'} + k_b^{\gamma\gamma'}). \end{aligned} \quad (2)$$

Here,  $\gamma$  and  $\gamma'$  represent  $xy$ ,  $yz$  and  $zx$  orbitals and  $k_a^{xy,xy} = k_b^{xy,zx} = k_1$ ,  $k_b^{xy,xy} = k_a^{xy,zx} = k_2$ ,  $k_a^{yz,yz} = k_a^{xy,yz} = k_2$ ,  $k_b^{yz,yz} = k_b^{xy,yz} = -(k_1 + k_2)$ ,  $k_a^{zx,zx} = k_a^{yz,zx} = -(k_1 + k_2)$  and  $k_b^{zx,zx} = k_b^{yz,zx} = k_1$ , respectively. In Fig. 1, we show the band dispersions and the

Fermi surfaces obtained from  $H_{\text{kin.}} + H_{\text{cry.}}$  in the case of  $t_1 = 0.45$ ,  $t_2 = 0.05$ ,  $t_3 = 1$ ,  $t_4 = 0.2$ ,  $t_5 = -0.15$ ,  $t_6 = -0.05$ ,  $t_7 = 0.12$ ,  $t_8 = 0.12$ ,  $t_9 = -0.45$  and  $\Delta = 0.4$ . Both reproduce very well the LDA results [20], particularly near the Fermi level. In the following, we use these parameters and  $t_3 = 1$  as the energy unit.

As shown in Fig. 1, the Fermi surfaces consist of a large cylindrical one around the  $\Gamma$ -point and six hole pockets near the  $K$ -points. The cylindrical Fermi surface has a dominant  $a_{1g}$ -orbital character, while the six hole pockets have an  $e'_g$ -orbital character. Koshiba and Maekawa [24] discussed hidden Kagome lattices using the second-nearest neighbor hoppings. However, in their case, the obtained Fermi surfaces have six large hole pockets around the  $M$ -points in contrast to the LDA result. It is essential to take into account up to the third nearest-neighbor hoppings for reproducing the LDA result.

The last term in  $H$ ,  $H_{\text{int.}}$  represents the on-site  $d$ - $d$  Coulomb interactions, where  $H_U$  and  $H_{U'}$  are the intra- and inter-orbital Coulomb interactions, respectively, and  $H_{J_H}$  and  $H_{J'}$  are the Hund's-rule coupling and the pair-hopping interactions, respectively. These interactions are expressed using Kanamori parameters,  $U$ ,  $U'$ ,  $J_H$  and  $J'$ , which satisfy the relations;  $U' = U - 2J_H$  and  $J_H = J'$ . The value of  $U$  has been estimated as 3-5.5 eV from the photoemission spectroscopy [25], and the value of  $J_H$  for the  $\text{Co}^{3+}$  ion is 0.84 eV. Thus, the ratio  $J_H/U$ , which gives the strength of Hund's-rule coupling, is 0.15-0.28 in this compound.

We analyze this multi-orbital Hubbard model by extending the FLEX approximation to the multi-orbital case. In the FLEX approximation, RPA-type bubble diagrams and ladder diagrams are taken into account. By determining self-consistently the renormalized Green's function and fluctuation exchange self-energy, the effects of mode-mode coupling between charge and spin fluctuations and quasi-particle damping due to these fluctuations are incorporated. In the present three-orbital case, the irreducible Green's function  $\hat{G}$ , the non-interacting Green's function  $\hat{G}^{(0)}$  and the self-energy  $\hat{\Sigma}$  are expressed in the  $3 \times 3$ -matrix form corresponding to the  $xy$ ,  $yz$  and  $zx$  orbitals. The irreducible, spin and charge-orbital susceptibilities ( $\hat{\chi}^0$ ,  $\hat{\chi}^s$  and  $\hat{\chi}^c$ ) as well as the effective interaction ( $\hat{V}$ ) have a  $9 \times 9$ -matrix form. Note that  $\hat{\chi}^c$  expresses the fluctuations of both charge and orbital degrees of freedom. The Green's function satisfies the Dyson-Gor'kov equation;

$$(1) \quad \hat{G}(k)^{-1} = \hat{G}^{(0)}(k)^{-1} - \hat{\Sigma}(k), \quad (3)$$

with

$$\Sigma_{mn}(k) = \frac{T}{N} \sum_q \sum_{\mu\nu} V_{\mu m, \nu n}(q) G_{\mu\nu}(k - q). \quad (4)$$

Here, the matrix element of the effective interaction is

given by

$$V_{mn,\mu\nu}(q) = \left[ \frac{3}{2} \hat{U}^s \hat{\chi}^s(q) \hat{U}^s + \frac{1}{2} \hat{U}^c \hat{\chi}^c(q) \hat{U}^c - \frac{1}{4} (\hat{U}^s + \hat{U}^c) \hat{\chi}^0(q) (\hat{U}^s + \hat{U}^c) + \frac{3}{2} \hat{U}^s - \frac{1}{2} \hat{U}^c \right]_{mn,\mu\nu} \quad (5)$$

The spin and charge-orbital parts of susceptibilities ( $\hat{\chi}^s$  and  $\hat{\chi}^c$ ) are

$$\hat{\chi}^s(q) = [\hat{I} - \hat{\chi}^0(q) \hat{U}^s]^{-1} \hat{\chi}^0(q), \quad (6)$$

$$\hat{\chi}^c(q) = [\hat{I} + \hat{\chi}^0(q) \hat{U}^c]^{-1} \hat{\chi}^0(q), \quad (7)$$

with the irreducible susceptibility

$$\chi_{mn,\mu\nu}^0(q) = -\frac{T}{N} \sum_k G_{\mu m}(k+q) G_{n\nu}(k). \quad (8)$$

In the above,  $T$  is temperature,  $k \equiv (\mathbf{k}, i\omega_n)$  and  $q \equiv (\mathbf{q}, i\nu_l)$  with  $\omega_n = (2n-1)\pi T$  and  $\nu_l = 2l\pi T$ ,  $N$  is the number of sites, and  $\hat{I}$  is a unit matrix. The interaction matrices  $\hat{U}^s$  and  $\hat{U}^c$  are represented as

$$\hat{U}^s = \begin{bmatrix} \hat{U}_1^s & \hat{0} \\ \hat{0} & \hat{U}_2^s \end{bmatrix}, \quad \hat{U}^c = \begin{bmatrix} \hat{U}_1^c & \hat{0} \\ \hat{0} & \hat{U}_2^c \end{bmatrix}. \quad (9)$$

where  $[\hat{U}_1^s]_{aa,bb}$  ( $[\hat{U}_1^c]_{aa,bb}$ ) is  $U$  ( $U$ ) for  $a = b$ , and  $J_H$  ( $2U' - J_H$ ) for  $a \neq b$ . On the other hand,  $[\hat{U}_2^s]_{ab,cd}$  ( $[\hat{U}_2^c]_{ab,cd}$ ) with  $a \neq b$  and  $c \neq d$  is given by  $U'$  ( $-U' + 2J_H$ ) for  $a = c$  and  $b = d$ , and is given by  $J'$  ( $J'$ ) for the other cases.

To discuss the nature of superconductivity, we solve the following Eliashberg equation;

$$\lambda \phi_{mn}(k) = -\frac{T}{N} \sum_q \sum_{\mu\nu} K_{mn,\mu\nu}^{\eta}(q) \phi_{\mu\nu}(k-q), \quad (10)$$

with

$$K_{mn,\mu\nu}^{\eta}(q) = \sum_{\alpha\beta} \Gamma_{\alpha m, n\beta}^{\eta}(q) G_{\alpha\mu}(k-q) G_{\beta\nu}(q-k). \quad (11)$$

The singlet and triplet pairing interactions  $\Gamma^s$  and  $\Gamma^t$  have 9×9-matrix forms as,

$$\hat{\Gamma}^s(q) = \frac{3}{2} \hat{U}^s \hat{\chi}^s(q) \hat{U}^s - \frac{1}{2} \hat{U}^c \hat{\chi}^c(q) \hat{U}^c + \frac{1}{2} (\hat{U}^s + \hat{U}^c), \quad (12)$$

$$\hat{\Gamma}^t(q) = -\frac{1}{2} \hat{U}^s \hat{\chi}^s(q) \hat{U}^s - \frac{1}{2} \hat{U}^c \hat{\chi}^c(q) \hat{U}^c + \frac{1}{2} (\hat{U}^s + \hat{U}^c). \quad (13)$$

The eigenvalue  $\lambda$  is a measure for the dominant superconducting symmetry, and becomes unity at  $T = T_c$ .

First, let us discuss the spin and charge fluctuations [26]. Figure 2 shows the spin susceptibility  $\chi^s$  obtained by solving Eqs. (3)-(9) self-consistently for various values of  $J_H/U$  at  $T = 0.02$ . Apparently, a peak structure around  $\Gamma$ -point is strongly enhanced as  $J_H/U$  increases, while the small peak at the M-point hardly changes [27]. Since the value of  $J_H/U$  is 0.15-0.28 in the actual compound, the enhanced peak at  $\Gamma$ -point at

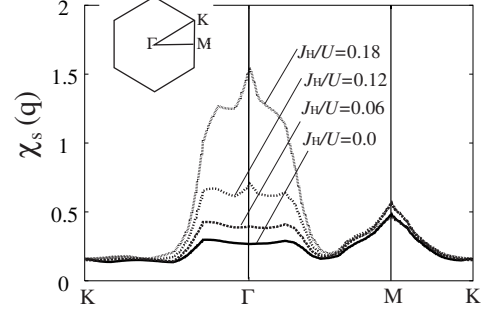


FIG. 2: Spin susceptibility  $\chi^s$  showing the evolution of FM fluctuation, as the strength of Hund's-rule coupling  $J_H/U$  increases.

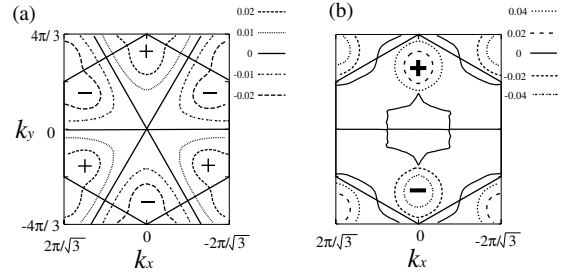


FIG. 3:  $k$ -dependence of the superconducting gaps with the largest  $\lambda$ : (a)  $f_{y(y^2-3x^2)}$ -wave gap and (b)  $p_y$ -wave gap.

$J_H/U = 0.18$  indicates that the FM fluctuation is dominant in this compound. As mentioned before, FM spin fluctuation has been observed experimentally [4, 5, 22]. On the other hand, the charge-orbital susceptibility  $\chi^c$  does not exhibit any remarkable structures, which implies an absence of charge- and orbital-density-wave instabilities.

By solving the Eliashberg equations, we find that triplet  $f_{y(y^2-3x^2)}$ -wave or  $p$ -wave pairings have the largest  $\lambda$  in the calculated parameter region of  $0 < J_H/U < 0.30$ . Although the values of  $\lambda$  are nearly the same,  $\lambda$  for  $f_{y(y^2-3x^2)}$ -wave state is slightly larger in the region of  $J_H/U < 0.2$  while  $\lambda$  for  $p$ -wave state is larger in  $J_H/U > 0.2$ . The other pairing instabilities are considerably weak. We have also studied a second-order perturbation theory and have obtained consistent results [28].

Figure 3 shows the  $k$ -dependence of the obtained superconducting gaps with (a)  $f_{y(y^2-3x^2)}$ -wave and (b)  $p$ -wave symmetries. As for the  $p$ -wave gap, the  $p_y$  state is shown among the twofold degenerate  $p_x$  and  $p_y$  states. Below  $T_c$ , the  $p$ -wave gap is represented as  $\sqrt{\Delta_x(k)^2 + \Delta_y(k)^2}$  with  $\Delta_x(k)$  ( $\Delta_y(k)$ ) being an order parameter for  $p_x$  ( $p_y$ ) state. This gap structure has line nodes on the  $a_{1g}$  Fermi surface since the line nodes of  $p_x$  and  $p_y$  states have nearly six-fold symmetry as shown in Fig. 3 (b). It is apparent that the magnitude of gap is large on the  $e'_g$  band with six hole-pocket Fermi surfaces. On the other hand, the amplitude of the gap on the  $a_{1g}$  band with a large cylindrical Fermi surface is

considerably small. The geometry of the Fermi surfaces plays a very important role: Because of the disconnectivity of the Fermi surfaces, the nodal lines run between the  $e'_g$  hole pockets and do not intersect them. Consequently, the gap is fully opened on each  $e'_g$  Fermi surface, while  $a_{1g}$  Fermi surface has line nodes. As discussed before the discovery of  $\text{Na}_{0.35}\text{CoO}_2\cdot 1.3\text{H}_2\text{O}$ , this kind of disconnectivity favors superconductivity by avoiding the disadvantage from nodes on the Fermi surface [29]. The dominant contribution of the  $e'_g$  band to the superconductivity is also attributed to the van Hove singularity (vHS) in the  $e'_g$  band. As can be seen in the band structure in Fig. 1, there exist saddle points near the K-points. This leads to a large density of states (DOS) near the Fermi level, which was actually reproduced in the LDA calculation [20].

Experimental estimate of the value of  $J_{\text{H}}/U$  has an ambiguity and is ranged from 0.15 to 0.28. Thus, both  $f_{y(y^2-3x^2)}$  state ( $J_{\text{H}}/U < 0.2$ ) and  $p$  state ( $J_{\text{H}}/U > 0.2$ ) can be candidates for the pairing state in the actual material. Now, let us discuss the present results with experiments. Both  $f$ -wave and  $p$ -wave gap structures obtained here are consistent with several NQR/NMR experiments [5, 6], which suggest existence of line nodes. Time-reversal symmetry observed in  $\mu\text{SR}$  [14] excludes the possibility of chiral  $p$ -wave state ( $p_x + ip_y$ ). Furthermore, the recent measurements of Knight shift [22, 30] and  $H_{c2}$  [31, 32] are consistent if the  $d$ -vector is fixed to be parallel to the plane [33]. In the case of  $p$ -wave pairings,  $\hat{x}p_x - \hat{y}p_y$  and  $\hat{x}p_y - \hat{y}p_x$  states are consistent with the experiments. However, a contradictory result about the constant Knight shift below  $T_c$  has also been reported [4] so that further careful study is needed.

Our calculation shows that the  $e'_g$  hole pockets play a substantially important role for superconductivity. In fact, if we study the situation without these hole pockets by tuning the transfer parameters, we find that the pairing instability is strongly suppressed and the realization of superconductivity with  $T_c \sim 5$  K is difficult. So far, the angle-resolved photoemission spectroscopy has been performed for the non-hydrate material [8], and the pocket Fermi surfaces predicted in the LDA calculations have not been detected. This might be due to a surface effect or some matrix elements. On the other hand, the Fermi surfaces of hydrate material is not clear at present.

In summary, we have studied the spin and charge fluctuations and the superconductivity in  $\text{Na}_x\text{CoO}_2\cdot 1.3\text{H}_2\text{O}$  on the basis of the FLEX analysis of the multi-orbital Hubbard model. The Hund's-rule coupling between the Co  $t_{2g}$  orbitals is shown to give rise to the FM spin fluctuation in consistent with the NQR results from several groups [4, 5, 22]. The triplet pairing instability mediated by this FM fluctuation arises mainly on the  $e'_g$  band with the pocket Fermi surfaces. The hole-pocket Fermi surfaces as well as a large DOS due to the vHS near the Fermi level are crucially important for the superconductivity. We have pointed out that this material can be a first example of the inter-orbital-interaction-induced triplet superconductivity.

We thank K. Ishida, G.-q.Zheng, K. Yoshimura, K. Kobayashi, M. Sato, R. Kadono, K. Kuroki, G. Baskaran for valuable discussions. M.M also thanks S. Onari and Yasuhiro Tanaka for discussions. This work is supported by “Grant-in-Aid for Scientific Research” from the MEXT of Japan.

---

[1] K. Takada *et al.*, *Nature* **422**, 53 (2003).  
 [2] P.W. Anderson, *Mater Res. Bull.* **8**, 153 (1973).  
 [3] P.W. Anderson, *Science* **235**, 1196 (1987).  
 [4] T. Waki *et al.*, cond-mat/0306036.  
 [5] K. Ishida *et al.*, *J. Phys. Soc. Jpn.* **72**, 304 (2003).  
 [6] T. Fujimoto *et al.*, *Phys. Rev. Lett.* **92**, 047004 (2004).  
 [7] Y. Wang *et al.*, cond-mat/0305455.  
 [8] H.-B. Yang *et al.*, cond-mat/0310532.  
 [9] T. Koretsune and M. Ogata, *Phys. Rev. Lett.* **89**, 116401 (2002).  
 [10] G. Baskaran, *Phys. Rev. Lett.* **91**, 097003 (2003).  
 [11] B. Kumar and B.S. Shastry, *Phys. Rev. B* **68**, 104508 (2003).  
 [12] Q.H. Wang *et al.*, *Phys. Rev. B* **69**, 092504 (2004).  
 [13] M. Ogata, *J. Phys. Soc. Jpn.* **72**, 1839 (2003).  
 [14] W. Higemoto *et al.*, cond-mat/0310324.  
 [15] G. Baskaran, cond-mat/0306569.  
 [16] O. I. Motrunich and P. A. Lee, cond-mat/0310387.  
 [17] H. Ikeda *et al.*, *J. Phys. Soc. Jpn.* **73**, 17 (2004).  
 [18] Y. Nisikawa *et al.*, *J. Phys. Soc. Jpn.* **73**, 970 (2004).  
 [19] Y. Tanaka, Y. Yanase and M. Ogata, *J. Phys. Soc. Jpn.* **73**, 319 (2004).  
 [20] D. J. Singh, *Phys. Rev. B* **61**, 13397 (2000).  
 [21] M. D. Johannes and D. J. Singh, cond-mat/0401646.  
 [22] Y. Kobayashi *et al.*, *J. Phys. Soc. Jpn.* **72**, 2161 (2003).  
 [23] D. J. Singh, *Phys. Rev. B* **68**, 020503 (2003).  
 [24] W. Koshiba and S. Maekawa, *Phys. Rev. Lett.* **91**, 257003 (2003).  
 [25] A. Chainani *et al.*, cond-mat/0312293.  
 [26] Calculations are numerically carried out with  $32 \times 32$   $k$ -meshes in the first Brillouin zone, and 4096 Matsubara frequencies. The value of  $U$  is fixed at 6.0, and temperature  $T$  is fixed at 0.02.  
 [27] The peak at the M-point originates from the inter-hole-pocket scatterings with wavenumbers of  $q_1$  and  $q_2$  as shown in Fig. 1.  
 [28] Y. Yanase, M. Mochizuki and M. Ogata, in preparation.  
 [29] K. Kuroki and R. Arita, *Phys. Rev. B* **63**, 174507 (2001).  
 [30] K. Ishida, G.-q. Zheng and Y. Kitaoka, private communication.  
 [31] F.C. Chou *et al.*, cond-mat/0306659.  
 [32] T. Sasaki *et al.*, *J. Phys. Soc. Jpn.* **73**, 1131 (2004).  
 [33] Generally, the anisotropy of  $d$ -vector comes from the spin-orbit (LS) interaction as in  $\text{Sr}_2\text{RuO}_4$  [34]. Although the LS interaction is weaker in Co ( $3d$ ) than in Ru ( $4d$ ), we expect that the anisotropy appears in the lower order with respect to the LS coupling  $\lambda_{ls}$  than in  $\text{Sr}_2\text{RuO}_4$ . In  $\text{Sr}_2\text{RuO}_4$ , the mixing between the  $t_{2g}$  orbitals is weak so

that the anisotropy appears only from  $\lambda_{ls}^2$  order, while in  $\text{Na}_{0.35}\text{CoO}_2 \cdot 1.3\text{H}_2\text{O}$ , the mixing of orbitals is strong and the anisotropy appears from  $\lambda_{ls}$ -linear order.

[34] Y. Yanase and M. Ogata, *J. Phys. Soc. Jpn.* **72**, 673 (2003).